IEEE INSTRUMENTATION & MEASUREMENT SOCIETY

Received 17 June 2022; revised 15 August 2022; accepted 26 August 2022. Date of publication 12 September 2022; date of current version 29 September 2022.
The review of this article was arranged by Associate Editor Min Xia.

Digital Object Identifier 10.1109/OJIM.2022.3205672

An Efficient Phenomenological Inversion Method for Reconstruction of Crack Depth Profile in a Metal From ACFM Probe Output Signals

TEIMOUR HEIDARI AND SEYED HOSSEIN HESAMEDIN SADEGHI, (Senior Member, IEEE)

Department of Electrical Engineering, Amirkabir University of Technology, Tehran 15914, Iran

CORRESPONDING AUTHOR: S. H. H. SADEGHI (e-mail: sadeghi@aut.ac.ir)

ABSTRACT This article proposes an efficient phenomenological inversion method to determine the depth profile of a surface-breaking crack in a metal from the output signal of an alternating current field measurement (ACFM) probe. The proposed method utilizes a conjugate gradient algorithm to minimize an objective function, representing the difference between the probe predicted and actual signals in an iterative manner. The objective function is derived explicitly in terms of crack depth variables by considering a polynomial function for the field distribution in the depth direction and applying appropriate Green's functions. This approach enhances the accuracy and computational efficiency of the inversion process, regardless of the choice of the initial crack depth profile or the presence of noise in the measurement system. The validity and efficiency of the proposed method are demonstrated by comparing the reconstructed depth profiles of several simulated and machine-made cracks with their actual data, and those obtained using the conventional phenomenological approach based on an efficient stochastic optimization scheme along with a fast pseudo-analytic ACFM probe output simulator.

INDEX TERMS Conjugate gradient algorithm, depth profile, eddy current (EC) testing, fatigue crack, phenomenological inversion method.

I. INTRODUCTION

THE EARLY detection and sizing of fatigue cracks in metallic elements can play an important role in the prevention of catastrophic structural collapse [1]. The formation of these cracks is often initiated from the metal surface where high-stress concentrations exist. They do not have a constant predetermined shape since their propagation is a stochastic process due to the inherent uncertainties originating from environmental conditions, cyclic mechanical loads, etc. The initial tiny cracks tend to join each other and form a longer crack with multiple-hump depth profile [2].

The ac field measurement (ACFM) technique, derived from the principle of eddy-current (EC) testing, is widely used for the detection and sizing of surface cracks in metals. In this technique, interrogating ECs are induced in the specimen under test by an alternating-current-carrying wire, and the resultant magnetic field variations around the crack are monitored with a magnetic field sensor [3], [4], [5], [6]. While sharing the merits of the conventional EC testing [7], the ACFM method offers additional features as follows. The output signal in the EC probe, measuring the changes in the impedance of the inducing coil, represents a global variation of magnetic field distribution around a crack, whereas an ACFM probe provides the actual magnetic field perturbations, containing more information about the crack. Besides, in the ACFM technique, the inducer and the sensor are separated from each other as opposed to the EC probe where the inducer is usually part of the sensing system. The separation of the inducer and the sensor enables one to examine various incident field distributions produced by arbitrary-shape inducers.

Like all other nondestructive evaluation (NDE) methods, the main objective in ACFM testing is solving the so-called inverse problem where information about the geometry of a crack (i.e., length, direction, and depth profile) is sought, using probe output signals. Although crack length and direction can be readily determined by performing a two-dimensional (2-D) scan of the specimen surface [8], the determination of the crack depth profile in a real-time

application requires an efficient solution to the inverse problem.

The methods for the solution of the inverse problem can be categorized into two different types, namely, algorithmic and phenomenological. In algorithmic methods, an appropriate signal processing technique is used to map the crack signal to its geometrical parameters. Calibration curves and artificial neural networks (ANNs) are typical algorithmic methods. Calibration curves are used to relate features of the crack signal to various parameters of crack geometry. Although this method can be accurate and fast, its application is limited to characterization of cracks with known geometries, such as long [9], [10], circular-arc [11], or rectangular [12]. For cracks with complex geometries, ANNs are often used to map the crack signal to its geometry parameters [8], [13], [14]. Despite its fast operation, the accuracy of an ANN depends largely on its proper training. Such a training procedure requires a large database of crack signals which is often difficult to obtain. Another issue is the deficiency of ANNs when experiencing noisy data, even in the presence of a large database of crack signals.

Phenomenological methods, on the other hand, use a physical model into an iterative inversion process for solving the problem. They require a crack signal simulator (i.e., forward problem solver) and an optimization algorithm that minimizes an objective function. The objective function is the difference between the measured crack signal and its model-reconstructed counterpart. When the objective function reaches a predetermined minimum value, the respective reconstructed crack depth profile will be considered as the solution.

There are two distinct methods that can be used to solve an optimization problem, namely, the stochastic and the gradient-based methods. In the stochastic methods, the solution in each iteration is improved by a systematic search algorithm that is performed within the solution data set. The search algorithm can be done heuristically by a variety of evolution strategies [15], [16], [17], [18], or more efficiently by a pattern search algorithm through a local exploration of the cost function on the points in the vicinity of the current solution [19].

The gradient-based optimization methods are preferred to their stochastic rivals that suffer from slow convergence speed due to their intrinsic time-consuming searching mechanisms [20]. In these methods, the gradient of the objective function is used to update the solution in each iteration [21], [22], [23], [24], [25]. The convergence speed and the avoidance of trapping in local minimums depend strongly on the number of equations and unknowns, the initial choice of solution, and how to calculate the gradient of the objective function. In other words, the merits of the gradient method may not be achieved if it is not implemented appropriately in the inverse problem at hand. For example, the objective function, representing the error between the predicted and actual probe output signals, includes multiple unknown electric and magnetic field variables, thus increasing the likelihood of trapping in local minimum points for noisy signals. In fact, one cannot obtain an explicit relation for the objective function in terms of the unknown parameters of the crack depth profile, although several pseudo-analytical forward problem solvers methods have been developed for various ACFM testing modalities [26], [27], [28], [29]. Besides, the computation of the error gradient in each iteration requires the solution of the forward problem which imposes additional computational costs.

Referring to the challenges described above, we propose an efficient phenomenological technique for reconstructing the depth profile of a surface-breaking crack in a metallic slab from the output signal of an ACFM probe. The proposed technique is based on an iterative inversion algorithm that utilizes a recently developed pseudo-analytical technique [29] in conjunction with a gradient-based optimization algorithm. By assuming a polynomial function for the field distribution in the depth direction and applying appropriate Green's functions, the objective function can be derived explicitly in terms of depth variables as a matrix equation. The crack depth profile is reconstructed by minimizing the objective function in an iterative fashion, using a conjugate gradient optimization algorithm. Since there is no need for a repetitive solution to the forward problem, the speed of convergence to global minimum points significantly increases. This feature can be more evident for noisy signals and improper choices of the initial depth profile.

The remainder of this article is organized as follows. The general formulation of the proposed inverse technique, including the derivation of the objective function and the implementation of the conjugate gradient optimization algorithm, is discussed in Section II. The validity and efficiency of the proposed technique are demonstrated in Section III where the actual and reconstructed depth profiles of several simulated and machine-made cracks with no predetermined geometries are compared.

II. FORMULATION

The geometry of the problem is shown in Fig. 1(a) where a conducting half space with conductivity σ_1 and permeability μ_1 contains a surface-breaking crack with an arbitrary depth profile along the x-axis. The two faces of the crack are perpendicular to the metal surface, lying in the direction of the x-axis, with very narrow opening g and length l.

The crack depth profile is specified by the depths of K discrete points $(d_1, d_2, \ldots, d_K)$ at the boundary of the crack separated by an equidistance of δx_k, shown in Fig. 1(b). An ACFM probe (containing a current-carrying wire inducer and a magnetic field sensor) scans the metal surface. The inducer is excited by an ac current source of frequency f and magnitude I. It induces ECs with an arbitrary skin depth in the metal, and the sensor measures the z-component of the magnetic field at the metal surface. The sensor is attached to the inducer and can move automatically along the x- and y-directions by the scanner, and manually in the z-direction.

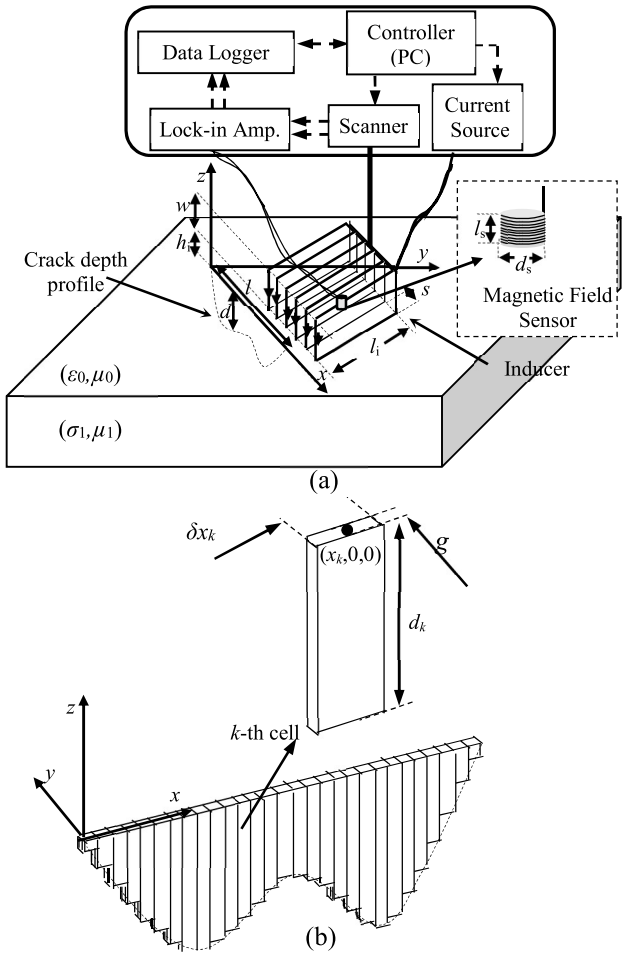

FIGURE 1. (a) ACFM probe (containing an inducer and a magnetic field sensor) scanning an arbitrary surface crack in a conductive specimen. (b) 1-D discretization of the crack with cubic cells.

The amplified amplitude and phase of the sensor output signal are measured by a lock-in amplifier and saved, using a digital data logger.

The aim is to provide an inverse modeling technique for the reconstruction of the crack depth from the sensor output signal. To this end, first, an initial depth profile is assumed. Then, an objective function is derived in terms of the crack depth variables $(d_1, d_2, \ldots, d_K)$ from the difference between the measured signal and the predicted signal of the initial crack. Finally, the depth profile of the crack is reconstructed by implementing a nonlinear conjugate gradient algorithm that minimizes the objective function.

A. OBJECTIVE FUNCTION

We start by discretizing the crack volume V_c into K cubic cells of dimensions $\delta x_k \times g \times d_k$ $(k = 1 : K)$, as shown in Fig. 1(b). Denoting the depth of the kth cell with d_k, the crack depth vector $\boldsymbol{d}$ is defined as follows:

$$\boldsymbol{d} = [d_1, d_2, \ldots, d_K]k = 1 : K. \tag{1}$$

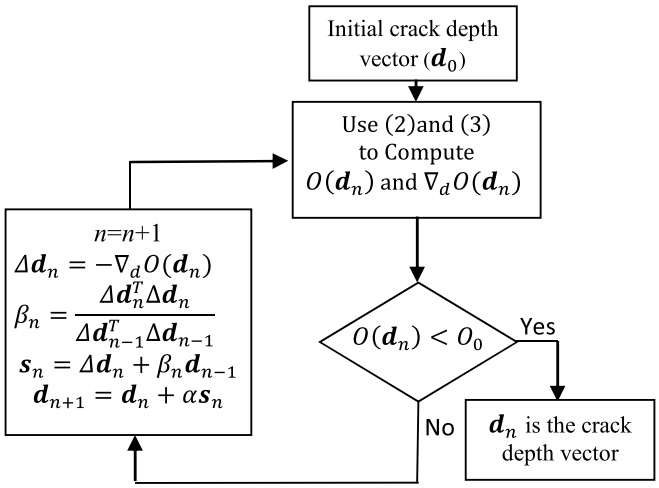

FIGURE 2. Proposed inversion method based on a conjugate gradient algorithm to determine the crack depth profile.

The objective function $O(\boldsymbol{d})$ and its gradient $\nabla_d O$ can be expressed as follows:

$$O(\boldsymbol{d}) = \sum_{j=1}^{J} \left\| h_{z_j}^{\text{prd}} - h_{z_j}^{\text{msr}} \right\|^2 \tag{2}$$

and

$$\nabla_d O = 2\text{Re} \sum_{k=1}^{K} \left(h_{z_j}^{\text{prd}} - h_{z_j}^{\text{msr}} \right)^* \nabla_d h_{z_j}^{\text{prd}} \tag{3}$$

where $h_{z_j}^{\text{msr}}$ and $h_{z_j}^{\text{prd}}$ denote the normalized sensor measured signal and its predicted signal at the point of j, respectively. The normalization factor is the sensor output signal in the absence of a crack; in practice, it is determined by measuring the sensor output signal in an area far from the crack, where a constant signal appears at the output of the detection system.

Taking advantage of the diffusion property of the electromagnetic field in the metal and based on the results of [29], the electric and magnetic field distribution in each element is assumed a second-degree polynomial for the z-dependence and pulse for the x- and y-dependence as follows and, hence, the electric and the magnetic fields inside the crack can be expressed as follows:

$$\boldsymbol{E}(\boldsymbol{r}) = \sum_{k=1}^{K} \chi_k(x, y, z) \left[\boldsymbol{a}_{2k} z^2 + \boldsymbol{a}_{1k} z + \boldsymbol{a}_{0k} \right] \tag{4a}$$

$$\boldsymbol{H}(\boldsymbol{r}) = \sum_{k=1}^{K} \chi_k(x, y, z) \left[\boldsymbol{b}_{2k} z^2 + \boldsymbol{b}_{1k} z + \boldsymbol{b}_{0k} \right] \tag{4b}$$

where

$$\chi_k(x, y, z) = \begin{cases} 1, & (x, y, z) \epsilon V_k \\ 0, & \text{else.} \end{cases} \tag{5}$$

Here, $(\boldsymbol{a}_{2_k}, \boldsymbol{a}_{1_k}, \boldsymbol{a}_{0_k})$ and $(\boldsymbol{b}_{2_k}, \boldsymbol{b}_{1_k}, \boldsymbol{b}_{0_k})$ are, respectively, the coefficients of the second-degree polynomials associated with E and H in the kth cell.

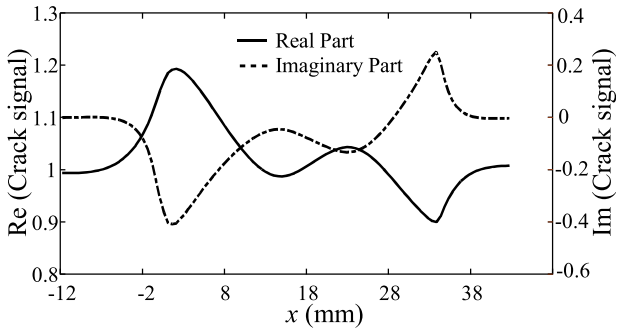

FIGURE 3. Variations of the crack signal h_z, when scanning the crack specified in Fig. 4 along line $y = -0.2$ mm at a lift distance $z_S = 0.2$ mm.

Using the half-space Green's functions, the electric and magnetic fields can be obtained everywhere as follows:

$$\begin{aligned}\boldsymbol{E}^{\mathrm{prd}}(\boldsymbol{r}) &= \boldsymbol{E}^{\mathrm{inc}}(\boldsymbol{r}) \\ &+ g\sum_{k=1}^{K}\int_{z'=0}^{d_k}\Big\{\overline{\boldsymbol{G}}^{\mathrm{ej}}(\boldsymbol{r},\boldsymbol{r}')\Big[\boldsymbol{a}_{2k}z'^2+\boldsymbol{a}_{1k}z'+\boldsymbol{a}_{0k}\Big] \\ &+ \overline{\boldsymbol{G}}^{\mathrm{em}}(\boldsymbol{r},\boldsymbol{r}')\Big[\boldsymbol{b}_{2k}z'^2+\boldsymbol{b}_{1k}z'+\boldsymbol{b}_{0k}\Big]\Big\}d\boldsymbol{z}' \\ k &= 1,2,\ldots,K \end{aligned} \tag{6a}$$

$$\begin{aligned}\mathbf{H}^{\mathrm{prd}}(\mathbf{r}) &= \mathbf{H}^{\mathrm{inc}}(\mathbf{r}) \\ &+ g\sum_{k=1}^{K}\int_{z'=0}^{d_k}\Big\{\overline{\mathbf{G}}^{\mathrm{hj}}(\mathbf{r},\mathbf{r}')\Big[\mathbf{a_{2k}}z'^2+\mathbf{a}_{1k}z'+\mathbf{a}_{0k}\Big] \\ &+ \overline{\mathbf{G}}^{\mathrm{hm}}(\mathbf{r},\mathbf{r}')\Big[\mathbf{b_{2k}}z'^2+\mathbf{b}_{1k}z'+\mathbf{b}_{0k}\Big]\Big\}\mathrm{d}z' \\ k &= 1,2,\ldots,K \end{aligned} \tag{6b}$$

where $\boldsymbol{r}$ and $\boldsymbol{r}'$ are the position vectors of observation (x, y, z) and source (x', y', z') points, respectively. The subscript "inc" denote the induced field in the absence of the crack (the incident field). Also, $\overline{\mathbf{G}}^{\mathrm{ej}}$ and $\overline{\boldsymbol{G}}^{\mathrm{em}}$ represent, respectively, the half-space electric dyadic Green's functions due to electric and magnetic current sources, and $\overline{\boldsymbol{G}}^{\mathrm{hj}}$ and $\overline{\boldsymbol{G}}^{\mathrm{hm}}$ represent, respectively, the half-space magnetic dyadic Green's functions due to electric and magnetic current sources. The derivation of the incident fields and the half-space electric dyadic Green's functions are detailed in [29]. According to (4a) and (4b), the coefficients of the second-degree polynomials in each cell can be derived from the fields of that cell as follows:

$$\boldsymbol{a}_{0k} = \boldsymbol{E}(x_k, 0, 0) \tag{7a}$$

$$\boldsymbol{a}_{1k} = \frac{\partial \boldsymbol{E}(x_k, 0, z)}{\partial z}|_{z=0} \tag{7b}$$

$$\boldsymbol{a}_{2k} = \frac{\partial^2 \boldsymbol{E}(x_k, 0, z)}{2\partial z^2}|_{z=0} \tag{7c}$$

$$\boldsymbol{b}_{0k} = \boldsymbol{H}(x_k, 0, 0) \tag{7d}$$

$$\boldsymbol{b}_{1k} = \frac{\partial \boldsymbol{H}(x_k, 0, z)}{\partial z}|_{z=0} \tag{7e}$$

$$\boldsymbol{b}_{2k} = \frac{\partial^2 \boldsymbol{H}(x_k, 0, z)}{2\partial z^2}|_{z=0}. \tag{7f}$$

TABLE 1. Comparison of the proposed method and its counterpart [19] when using various initial crack depth profiles shown in Fig. 4(a)–(d) to reconstruct the respective crack depth profiles, using the simulated crack signal given in Fig. 3.

Initial Crack Depth Profile	Proposed Method		Method of [19]	
	RMSD (%)	CPU Time (Sec)	RMSD (%)	CPU Time (Sec)
Fig. 4 (a)	9.9	9.5	15.6	65
Fig. 4 (b)	9.3	9.2	14.8	60
Fig. 4 (c)	7.1	6.8	9.5	48
Fig. 4 (d)	6.2	6	8.2	39

TABLE 2. Comparison of the proposed method and its counterpart [19] when using the simulated crack signals given in Fig. 6 to reconstruct the crack depth profiles shown in Fig. 7.

SNR (dB)	Proposed Method		Method of [19]	
	RMSD (%)	CPU Time (Sec)	RMSD (%)	CPU Time (Sec)
10	12.2	9.3	21.2	55.3
12	10.3	8.5	17	50.7
16	8.8	7.9	13.3	44.2
25	7.1	6.8	9.4	40.3

By combining the matrix equations obtained from (6) and (7), and eliminating the coefficients of the second-degree polynomials, the sensor-predicted signal can be obtained as a matrix relation, i.e.,

$$\left[h_z^{\mathrm{prd}}\right] = [A]\left[C^{\mathrm{inc}}\right] \tag{8}$$

where matrix $[C^{\mathrm{inc}}]$ contains the incident fields and their derivatives that are known. Matrix $[A]$ contains only the unknown variables of crack depth that appear at the boundaries of the integrals.

By substituting (8) in (2) and (3), the objective function and its gradient are obtained in terms of the crack depth vector. To determine the crack depth variables, we need to minimize the optimization problem posed in (2). This is done by resorting to the conjugate gradient method.

B. IMPLEMENTATION OF THE CONJUGATE GRADIENT METHOD

The conjugate gradient method is the most prominent gradient-based optimization method for its high convergence speed [30]. Using this method, the algorithm shown in Fig. 2 is developed to minimize the objective function in (2) by updating the crack depth vector $\boldsymbol{d}$ in an iterative manner. Referring to Fig. 2, the proposed algorithm starts by assigning the initial values of the crack depth vector d_0. It then follows an iterative procedure where the vector of the unknown depth profile at the nth iteration, $\boldsymbol{d}_n$, is used to obtain the respective value of the objective function, $O(\boldsymbol{d}_n)$. Provided that the value of $O(\boldsymbol{d}_n)$ is less than a predetermined threshold value O_0, the algorithm stops and the elements of $\boldsymbol{d}_n$ will be the estimated values of the crack depth vector. Otherwise, $\boldsymbol{d}_n$ is updated to obtain a new value of the objective function in the next iteration as follows:

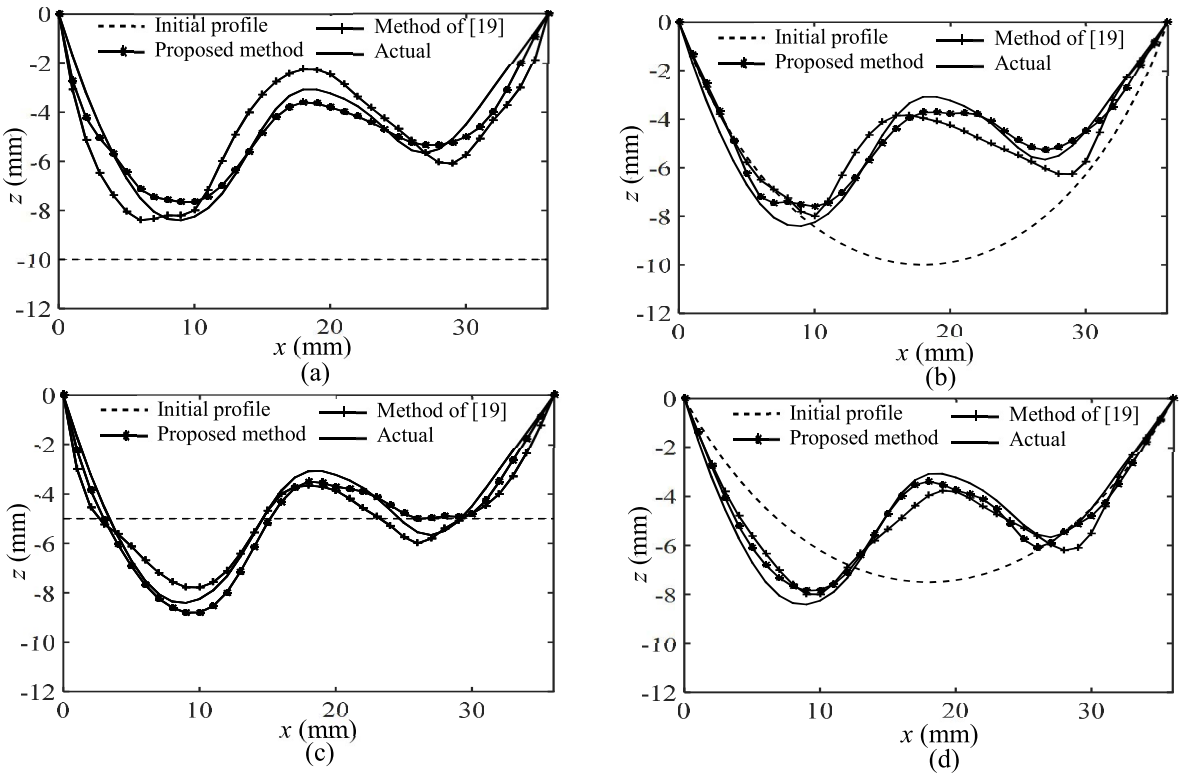

FIGURE 4. Actual and reconstructed crack depth profiles, using the crack signals shown in Fig. 3 and various initial crack depth profiles; (a) rectangular and (b) circular-arc cracks with a predetermined maximum sizable depth (10 mm), and (c) rectangle and (d) circular-arc cracks whose depths are determined such that the difference between the actual and predicted probe signals becomes minimum in the least squares sense.

$$\Delta \boldsymbol{d}_n = -\nabla_d O(\boldsymbol{d}_n) \tag{9a}$$

$$\beta_n = \frac{\Delta \boldsymbol{d}_n^T \Delta \boldsymbol{d}_n}{\Delta \boldsymbol{d}_{n-1}^T \Delta \boldsymbol{d}_{n-1}} \tag{9b}$$

$$\boldsymbol{s}_n = \Delta \boldsymbol{d}_n + \beta_n \boldsymbol{d}_{n-1} \tag{9c}$$

$$\boldsymbol{d}_{n+1} = \boldsymbol{d}_n + \alpha \boldsymbol{s}_n \tag{9d}$$

where coefficient α is an adjustable step length and its appropriate value is obtained by performing a line search [30]. Also, the value of O_0 is determined as follows:

$$O_0 = \tau^2 \sum_{j=1}^{J} \left\| h_{z_j}^{\text{msr}} \right\|^2 \tag{10}$$

where τ is a prespecified value representing the acceptable relative mean square error between the predicted and measured crack signals.

III. RESULTS

To evaluate the accuracy and computation performance of the proposed method, the results of various simulation and experimental tests are investigated. We also compare the results of the proposed method with those obtained using the method presented in [19]. The rival method in [19] adopts a phenomenological approach where an efficient stochastic optimization scheme along with a fast pseudo-analytic ACFM probe output simulator is utilized to predict the crack depth profile.

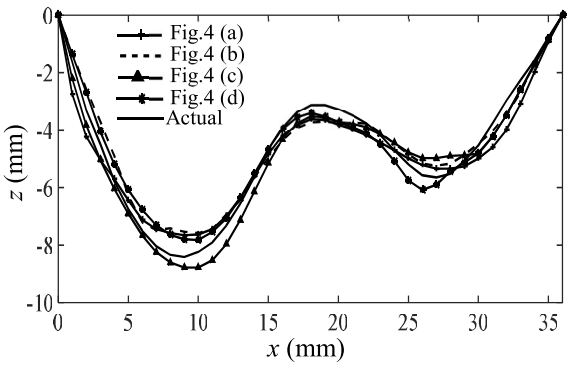

FIGURE 5. Reconstructed crack depth profiles, using the proposed method applied to the measured crack signals shown in Fig. 3 for various initial crack depth profiles in Fig. 4.

Referring to Fig. 1, the ACFM probe consists of a magnetic field sensor attached to an N-turn solenoid inducer with a rectangular cross section. It interrogates the surface of a metal slab containing a surface-breaking crack with an arbitrary depth profile. The sensor is a tiny pickup coil that measures the magnetic field h_z, of the surface point by point. The center of the sensor (x_s, y_s, z_s) is placed at a fixed position $(\Delta x_o, \Delta y_o, \Delta z_o)$ with respect to the center of the inducer.

The validity of the proposed method in all cases is quantitatively evaluated by examining the root mean square deviation (RMSD) between the actual crack depth profile,

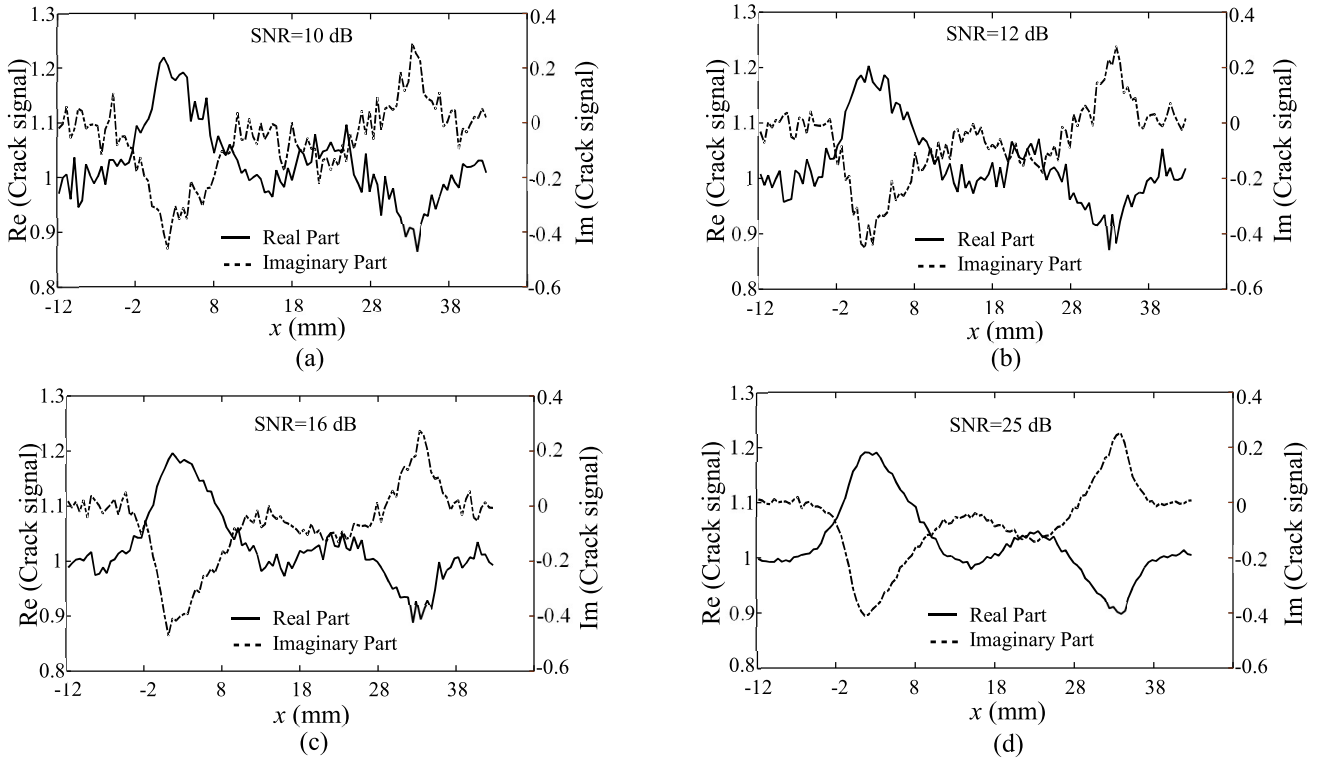

FIGURE 6. Variations of the crack signals, h_z, superposed by additive white Gaussian noise with SNRs when scanning the crack specified in Fig. 4 along line $y = -0.2$ mm and $z_s = 0.2$ mm; (a) SNR = 10 dB, (b) SNR = 12 dB, (c) SNR = 16 dB, and (d) SNR = 25 dB.

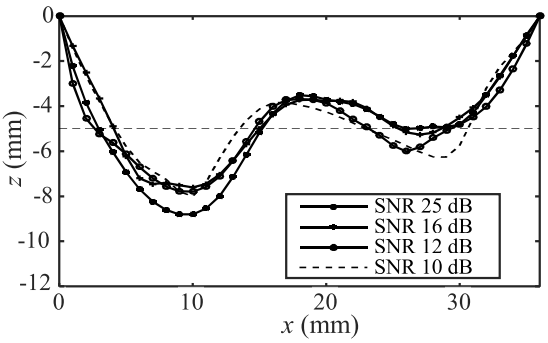

FIGURE 7. Reconstructed crack depth profiles, using the crack signals shown in Fig. 6 (a)–(d).

d_k $(k = 1, 2, \ldots, K)$, and its reconstructed counterpart, $\hat{d}_k$ $(k = 1, 2, \ldots, K)$, in all cases is given

$$\text{RMSD} = \sqrt{\frac{\sum_{k=1}^{K}\left(d_k^2 - \hat{d}_k^2\right)}{\sum_{k=1}^{K} d_k^2}}. \tag{11}$$

A. SELECTION OF THE INITIAL CRACK DEPTH PROFILE

In the first set of results, we present the simulated results (Fig. 3) of the case where the ACFM probe ($N = 3, l_i =$ 24 mm, $s = 5$ mm, and $w = 15$ mm, $f = 200$ Hz and $I = 1$ A) scans an aluminum metal, containing a two-hump arbitrary-shape crack (Fig. 4). The z-component of the magnetic field, h_z is measured by an induction coil magnetic

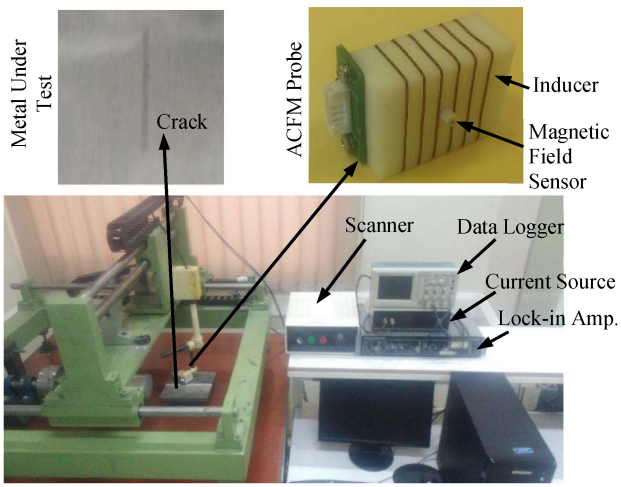

FIGURE 8. Experimental set up where an ACFM probe (comprising a rectangular inducer and a pickup coil magnetic field sensor) interrogates the surface of a metal slab with an arbitrary-shape surface crack.

field sensor that is placed at a fixed position ($\Delta x_o = 0$, $\Delta y_o = -2$ mm, and $\Delta z_o = -12.3$ mm) with respect to the center of the inducer.

To study how the initial crack depth profile affects the efficiency of the proposed method, four cases are examined. These are: 1) a rectangular and 2) a circular-arc cracks with a predetermined maximum sizable depth, and 3) a rectangle and 4) a circular-arc cracks with a depth that is determined such that the difference between the actual and predicted

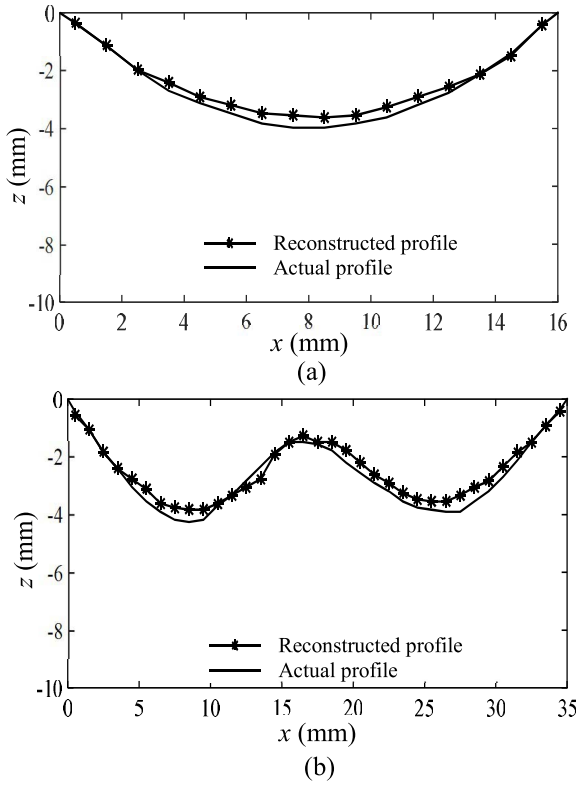

FIGURE 9. Actual and reconstructed depth profiles of two machine-made cracks with opening $g = 0.2$ mm; (a) single-hump depth profile and (b) double-hump depth profile.

probe signals become minimum in the least squares sense. It is worth noting that the crack length can be readily determined by a 2-D scan of the metal surface as large discernible rises and falls appear in the signal from at the two ends of the crack [8]. The crack signal (Fig. 3) is used to reconstruct the crack shape, using various initial crack depth profiles. A study of the results shown in Figs. 4 and 5 demonstrates the capability of the proposed method for accurate crack reconstruction, regardless of the choice of the initial depth profile. For comparison purposes, the values of RMSD and CPU times required for computation of the results on an Intel Core i3-370M Processor (3M cache, 2.40 GHz) with 8 GB of RAM (running MATLAB software package) are shown in Table 1. The values of RMSD in this table indicate that the circular-arc profile (offering the closest signal to the actual crack signal) is the best initial guess in the reconstruction process. A further study of the results in Table 1 demonstrates the superiority of the proposed method to its rival [19] both in terms of accuracy and computation efficiency. This is due to the fact that the forward problem in the method of [19] must be fully solved in each iteration, requiring a 2-D discretization of the crack face. This is in contrast with the proposed method where the problem is formulated in terms of the crack depth variables, requiring a 1-D discretization of the crack depth profile with a relatively smaller number of unknowns.

TABLE 3. Computational parameters for reconstruction of two machine-made cracks from ACFM probe output signals.

	single -hump crack	double -hump crack
Number of Cells	16	35
Time	3.8	6.1
RMSD	6.9%	8.7%

B. RESILIENCY TO NOISE

In practice, the probe output signal is always noisy. This is due to the inevitable electronic noise in the measurement circuitry and variations in the sensor lift-off as a result of fluctuations in probe mechanical movement. To evaluate the robustness of the proposed method in the presence of noise, the crack signal is superimposed by Gaussian noise with various signal-to-noise ratios (SNRs), as shown in Fig. 6.

The noisy crack signals are used to reconstruct the crack depth profile estimation when the rectangular crack in Fig. 4(c) is selected as the crack initial depth profile. A study of the reconstructed crack depth profiles (Fig. 7) further demonstrates the validity of the proposed inversion method. As expected, both the proposed method and its rival tend to deteriorate as the value of SNR decreases. This is clearly seen in the respective values of RMSD given in Table 2. A further study of the results in Table 2 shows that as the value of SNR is reduced from 25 to 10 dB, the value of RMSD in the proposed method increases from 7.1% to 12.2% (5.1% increase), whereas it increases from 9.4% to 21.4% (11% increase) in the case when the method of [19] is used. In other words, the proposed method appears to be more resilient to noise than its rival.

C. EXPERIMENTAL RESULTS

To further evaluate the performance of the proposed method, the setup shown in Fig. 8 is used. The setup consists of a motorized 2-D scanner, a current source, an ACFM probe (consisting of an inducer and a magnetic field sensor), a lock-in amplifier, and a digital data logger, all of which are controlled by a personal computer. The inducer, connected to the current source, induces ECs with a frequency of 80 Hz in the test block. It consists of six turns ($N = 6$) of 1-mm diameter copper wire with $l_i = 24$ mm, $s = 5$ mm, and $w = 15$ mm and is placed at a distance $h_i = 5$ mm above the metal surface. The magnetic field disturbed by the crack is measured at a speed of two samples per second by a tiny pickup coil sensor, consisting of 5 turns of 0.1-mm diameter copper wire uniformly wound on a cylindrical glass holder whose length and diameter are $l_s = 0.4$ mm and $d_s = 0.4$ mm, respectively. Because of the small size of the sensor, it essentially produces a point measurement of the magnetic field distribution. The center of the sensor (x_s, y_s, z_s) is placed at a fixed position ($\Delta x_o = 0$, $\Delta y_o = -0.7$ mm, and $\Delta z_o = -12.1$ mm) with respect to the center of the inducer and its axis is chosen to be perpendicular to the metal surface in order to measure the z-component of the magnetic field. The sensor is attached to the inducer and can move along the x- and y-directions by the scanner, and in the z-direction, by hand. The amplified

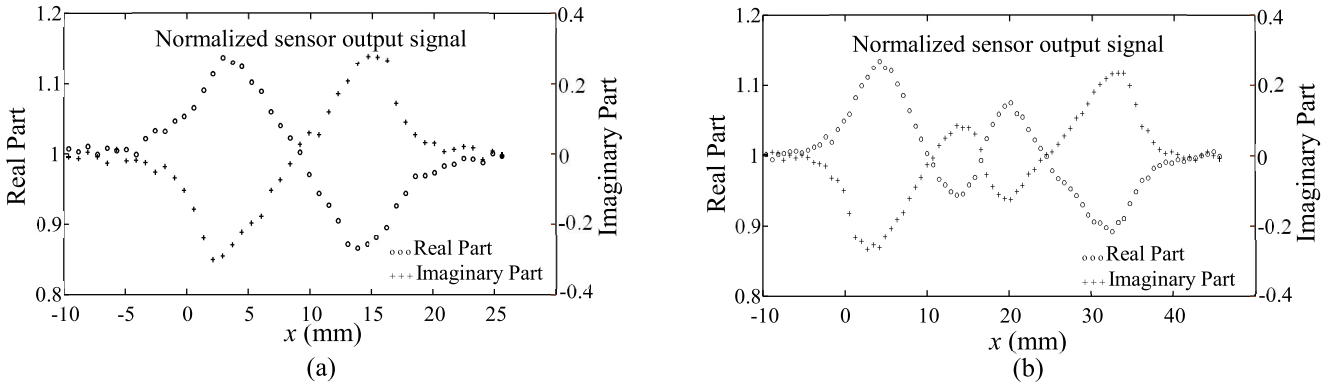

FIGURE 10. Normalized output signals of the ACFM probe when scanning the metal surface parallel to the crack edge along $y = -0.2$ mm and $z_S = 0.4$ mm; (a) crack with single-hump depth profile [Fig. 9(a)] and (b) crack with double-hump depth profile [Fig. 9(b)].

amplitude and phase of the sensor output signal are measured by the lock-in amplifier and saved in the digital data logger.

Two steel test blocks ($\mu_r = 100$ and $\sigma = 6 \times 10^6$ S/m), each containing a surface crack with no geometrical shape (Fig. 9), are used. The cracks have been manufactured by the electric discharge machinery technique [31]. Fig. 10 illustrates variations of the normalized sensor output signal associated with the two cracks when scanning the metal surface parallel to the crack edge at a lift-off distance $z_s = 0.4$ mm and $f = 80$ Hz. As can be seen in Fig. 10, there are discernible rises and falls in the sensor output signals when encountering the two ends of the cracks from which their lengths can be determined. Fig. 9 shows the response of the proposed inverse model for reconstructing the crack depth profile from the sensor output signals. A comparison of the actual crack depth profiles and their respective reconstructed counterparts demonstrates the accuracy of the proposed inversion technique. From the figures in Table 3, the value of RMSD in two cases is less than 9%, which indicates the good closeness of the reconstructed depth profiles with their respective actual counterparts.

IV. CONCLUSION

An efficient method has been proposed to reconstruct the depth profile of a surface-breaking crack in a metal by inverting the output signal of an ACFM probe. The proposed method is based on a phenomenological inversion method that adopts a gradient-based optimization algorithm to minimize the difference between the measured crack signal and its predicted counterpart in an iterative manner. The main feature of the proposed technique is its accurate and fast convergence for different choices of initial profile and noisy signals. This stems from the explicit relation derived for the objective function in terms of crack depth variables and the small dimensions of the resultant matrices in the inversion process. The validity and efficiency of the proposed technique have been demonstrated by reconstructing the depth profile of several simulated and machine-made cracks (with no predetermined geometries) in magnetic/nonmagnetic metallic blocks.

The proposed method can also be used to treat cracks with a nonstraight narrow opening. Besides, the scanning direction need not be along the crack opening. The only prerequisite is knowing the scan direction (with respect to the crack opening) to predict the sensor output signal in each iteration.

REFERENCES

[1] R. I. Stephens, *Metal Fatigue in Engineering*. New York, NY, USA: Wiley, 2001.

[2] W. D. Dover, R. Collins, R. B. Thompson, and D. H. Michael, "The use of AC-field measurement for crack detection and sizing in air and underwater," *Philos. Trans. Royal Soc. London A, Math. Phys. Sci.*, vol. 320, no. 1554, pp. 271–283, 1986.

[3] M. Lewis, D. H. Michael, M. C. Lugg, and R. Collins, "Thin-skin electromagnetic fields around surface breaking cracks in metals," *J. App. Phys.*, vol. 64, no. 8, pp. 3777–3784, Oct. 1988.

[4] D. Mirshekar-Syahkal, and R. F. Mostafavi, "1-D probe array for ACFM inspection of large metal plates," *IEEE Trans. Instrum. Meas.*, vol. 51, no. 2, pp. 374–382, Apr. 2002.

[5] J. Jun, J. Hwang, and J. Lee, "Quantitative nondestructive evaluation of the crack on the austenite stainless steel using the induced eddy current and the Hall sensor array," in *Proc. IEEE Instrum. Meas. Technol. Conf.*, May 2007, pp. 1–6.

[6] G. Betta, L. Ferrigno, and M. Laracca, "GMR-based instrument for ECT on conductive planar specimens," in *Proc. IEEE Instrum. Meas. Technol. Conf.*, May 2010, pp. 845–849.

[7] N. Bowler, *Eddy-Current Nondestructive Evaluation*. New York, NY, USA: Springer Nat., 2019.

[8] M. Ravan, S. H. H. Sadeghi, and R. Moini, "Neural network approach for determination of Fatigue crack depth profile in a metal, using alternating current field measurement data," *IET Sci. Meas. Technol.*, vol. 2, no. 1, pp. 32–38, Jan. 2008.

[9] S. H. H. Sadeghi and D. Mirshekar-Syahkal, "A method for sizing long surface cracks in metals based on the measurement of the surface magnetic field," in *Review of Progress in Quantitative Nondestructive Evaluation*. vol. 9A. New York, NY, USA: Plenum, 1990, pp. 351–358.

[10] S. H. H. Sadeghi, B. Toosi, and R. Moini, "On the suitability of induction coils for crack detection and sizing in metals by the surface magnetic field measurement technique," *NDT E Int.*, vol. 34, no. 7, pp. 493–504, 2001.

[11] S. H. H. Sadeghi and D. Mirshekar-Syahkal, "Scattering of an induced field by fatigue cracks in ferromagnetic metals," *IEEE Trans. Magn.*, vol. 28, no. 2, pp. 1008–1016, Mar. 1992.

[12] M. O. Ravari, S. H. H. Sadeghi, R. M. Mazandaran, and W. H. A. Schilders, "Field distributions around a rectangular crack in a metallic half space excited by long current-carrying wires with arbitrary frequency," *IEEE Trans. Magn.*, vol. 49, no. 3, pp. 1008–1018, Mar. 2013.

[13] J. A. Buck, P. R. Underhill, J. E. Morelli, and T. W. Krause, "Simultaneous multi parameter measurement in pulsed eddy current steam generator data using artificial neural networks," *IEEE Trans. Instrum. Meas.*, vol. 65, no. 3, pp. 672–679, Mar. 2016.

[14] L. S. Rosado, F. M. Janeiro, P. M. Ramos, and M. Piedade, "Defect characterization with eddy current testing using nonlinear-regression feature extraction and artificial neural networks," *IEEE Trans. Instrum. Meas.*, vol. 62, no. 5, pp. 1207–1214, May 2013.

[15] S. M. Ahmadkhah, R. P. R. Hasanzadeh, and M. Papaelias, "Arbitrary crack depth profiling through ACFM data using type-2 fuzzy logic and PSO algorithm," *IEEE Trans. Magn.*, vol. 55, no. 2, pp. 1–10, Feb. 2019.

[16] R. P. R. Hasanzadeh, S. H. H. Sadeghi, M. Ravan, A. Moghaddamjoo, and R. Moini, "A fuzzy alignment approach to sizing surface cracks by the AC field measurement technique," *NDT E Int.*, vol. 44, no. 1, pp. 75–83, Jan. 2011.

[17] N. Biju, N. Ganesan, C. V. Krishnamurthy, and K. Balasubramaniam, "Defect sizing simulation studies for the tone-burst eddy current thermography using genetic algorithm based inversion," *J. Nondestruct. Eval.*, vol. 31, no. 4, pp. 342–348, Jun. 2012.

[18] A. Noroozi, R. P. R. Hasanzadeh, and M. Ravan, "A fuzzy learning approach for identification of arbitrary crack profiles using ACFM technique," *IEEE Trans. Magn.*, vol. 49, no. 9, pp. 5016–5027, Sep. 2013.

[19] A. A. Khezri and S. H. H. Sadeghi, "Determination of crack depth profile in cylindrical metallic structures, using alternating current field measurement data," *J. Nondestruct. Eval.*, vol. 38, p. 57, May 2019.

[20] S. Koziel and X. S. Yang, *Computational Optimization, Methods and Algorithms*. Berlin, Germany: Springer, 2011.

[21] Z. Badics, H. Komatsu, K. Aoki, and Y. Matsumoto, "Inversion scheme based on optimization for 3-D eddy current flaw reconstruction problems," *J. Nondestruct. Eval.*, vol. 17, pp. 67–78, Jun. 1998.

[22] Z. Chen and K. Miya, "ECT inversion using a knowledge-based forward solver," *J. Nondestruct. Eval.*, vol. 17, pp. 167–175, Sep. 1998.

[23] J. R. Bowler, "Thin-skin eddy-current inversion for the determination of crack shape," *Inst. Phys. Inverse Probl*. vol. 18, no. 6, pp. 1891–1905, Nov. 2002.

[24] H. Haddar, Z. Jiang, and M. K. Riahi, "A robust inversion method for quantitative 3D shape reconstruction from coaxial eddy current measurements," *J. Sci. Comput.*, vol, 70, pp. 29–59, Jul. 2017.

[25] Y. Zhao, G. Wei, J. Han, W. Cai, H. Chen, and Z. Chen, "Enhancement of crack reconstruction through inversion of eddy current testing signals with a new crack model and a deterministic optimization method," *Meas. Sci. Technol.*, vol. 33, no. 5, Feb. 2022, Art. no. 55011.

[26] M. Ravan, S. H. H. Sadeghi, and R. Moini, "Field distributions around arbitrary shape surface cracks in metals, induced by high-frequency alternating-current-carrying wires of arbitrary shape," *IEEE Trans. Magn.*, vol. 42, no. 9, pp. 2208–2214, Sep. 2006.

[27] T. Heidari, H. Seidfaraji, S. H. H. Sadeghi, and R. Moini, "A fast analysis technique for electromagnetic interaction of high-frequency AC current-carrying wires with arbitrary-shape cracks in ferrous metals," *IEEE Trans. Magn.*, vol. 49, no. 3, pp. 1101–1107, Mar. 2013.

[28] A. Akbari-Khezri, S. H. H. Sadeghi, and R. Moini, "Field distribution around surface cracks in metallic cylindrical structures excited by high-frequency current-carrying coils of arbitrary shape," *IEEE Trans. Magn.*, vol. 51, no. 2, pp. 1–10, Feb. 2015.

[29] T. Heidari and S. H. H. Sadeghi, "Output signal prediction of an eddy-current probe when scanning arbitrary-shape surface cracks in metals," *IEEE Trans. Instrum. Meas.*, vol. 69, no. 6, pp. 3761–3769, Jun. 2020.

[30] N. Andrei, *Nonlinear Conjugate Gradient Methods for Unconstrained Optimization*. Cham, Switzerland: Springer Nat., 2020.

[31] J. A. Mcgeough, *Advanced Methods of Machining*. London, U.K.: Chapman Hall, 1988.